RSC Advances

PAPER

View Article Online
View Journal | View Issue

Cite this: *RSC Adv.*, 2018, **8**, 13259

Synthesis and physical properties of brominated hexacene and hole-transfer properties of thin-film transistors†

Motonori Watanabe, *[a] Takaaki Miyazaki,[b] Toshinori Matsushima,*[acd] Junko Matsuda,[a] Ching-Ting Chein,[e] Masahiko Shibahara,[f] Chihaya Adachi, [abcdg] Shih-Sheng Sun,[e] Tahsin J. Chow*[eh] and Tatsumi Ishihara [ag]

Received 25th December 2017
Accepted 13th March 2018

DOI: 10.1039/c7ra13632c

rsc.li/rsc-advances

A halide-substituted higher acene, 2-bromohexacene, and its precursor with a carbonyl bridge moiety were synthesized. The precursor was synthesized through 7 steps in a total yield of 2.5%. The structure of precursor and thermally converted 2-bromohexacene were characterized by solid state NMR, IR, and absorption spectra, as well as by DFT computation analysis. It exhibited high stability in the solid state over 3 months, therefore can be utilized in the fabrication of opto-electronic devices. The organic thin-film transistors (OFETs) were fabricated by using 2-bromohexacene and parent hexacene through vaccum deposition method. The best film mobility of 2-bromohexacene was observed at 0.83 $cm^2\ V^{-1}\ s^{-1}$ with an on/off ratio of 5.0×10^4 and a threshold of −52 V, while the best film mobility of hexacene was observed at 0.076 $cm^2\ V^{-1}\ s^{-1}$ with an on/off ratio of 2.4×10^2 and a threshold of −21 V. AFM measurement of 2-bromohexacene showed smooth film formation. The averaged mobility of 2-bromohexacene is 8 fold higher than the non-substituted hexacene.

1. Introduction

Acenes are amongst the most representative hydrocarbons for analysing the physical properties of polycyclic hydrocarbon materials.[1] Along with the increase in the number of aromatic benzene rings, acenes exhibit a reduction of both the HOMO–LUMO gap and the reorganisation energy.[2] The chemistry of acenes higher than pentacene, particularly their open-shell characteristics[3] and high charge transport properties, has attracted considerable attentions. Hence, these compounds and their analogs[4] such thieonoacene based semiconductor[5] are suitable for use in organic electronic devices such as organic field-effect transistors.[6–8] The extended π-conjugation of higher acenes also induce an interesting phenomenon of singlet fission that can be used on light harvesting.[9] Bulky substituents can enhance the thermal and photo-stability of acenes by lowering the radical characteristic in the ground state.[10] The isolation of higher acenes, from hexacene to nonacene and derivatives, has been achieved by applying this strategy. The modification of physical properties of acenes in the solid state requires a crystal engineering approach; however, their isolation steps are either difficult or tedious in order to obtain qualified structures due to their high thermal and light sensitivity in solutions.[11,12] To overcome the difficulty, stable precursors of acenes are prepared first, which can then be converted to the corresponding acenes quantitatively in demand through either a thermal or a photo-driven process.[13,14] The synthesis of nonacene derivatives has been achieved by this approach utilising a diketone precursor through photo-induced transformation.[15] Recently, the dimer structure of heptacene was converted to heptacene *via* a thermal retro-cyclization reaction, therefore showing its feasibility for further processes.[16] The precursor method can be used to produce higher acenes in large quantity that is required to become usable materials. Acenes have certain valuable potential applications, such as organic semi-conductors,[17] singlet fission materials,[18,19] and organic biradical sources.[15]

Previously, our group has developed the method of producing higher acene molecules from either monoketone

[a]*International Institute for Carbon Neutral Energy Research, Kyushu University, 744 Motooka, Nishi-ku,, Fukuoka 819-0395, Japan. E-mail: mwata@i2cner.kyushu-u.ac.jp*
[b]*Education Center for Global Leaders in Molecular Systems for Devices, Kyushu University, 744 Motooka Nishi-ku, Fukuoka 819-0395, Japan*
[c]*Center for Organic Photonics and Electronics Research (OPERA), Kyushu University, 744 Motooka, Nishi-ku, Fukuoka, Japan*
[d]*Japan Science and Technology Agency (JST), ERATO, Adachi Molecular Exciton Engineering Project, 744 Motooka, Nishi-ku, Fukuoka 819-0395, Japan*
[e]*Institute of Chemistry, Academia Sinica, No. 128, Academia Road Sec 2, Nankang, Taipei 11529, Taiwan*
[f]*Division of Natural Sciences, Faculty of Science and Technology, Oita University, Dannoharu 700, Oita, Japan*
[g]*Department of Applied Chemistry, Faculty of Engineering, Kyushu University, Nishi-ku, Fukuoka 819-0395, Japan*
[h]*Department of Chemistry, Tunghai University, Taichung 40704, Taiwan*

† Electronic supplementary information (ESI) available: Absorption spectra, DFT results, XRD, and NMR data. See DOI: 10.1039/c7ra13632c

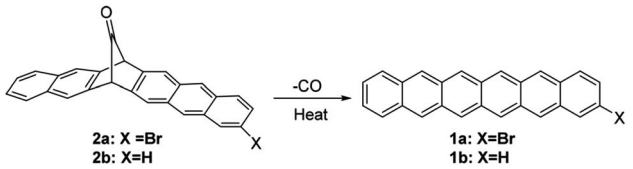

Fig. 1 The synthesis of 2-bromohexacene from its monoketone precursor.

precursors[20] or from diethylketomalonate precursors.[21] Both types of precursor can be cleanly converted to hexacene either thermally or photo-chemically. In addition, our group has generated halide-substituted tetracene[22] and pentacene[23] from their corresponding monoketone precursors. They were used successfully as the semiconductors in electronic devices. In these devices, single crystal bromopentacene device exhibits a significant superior hole mobility (>5 $cm^2 V^{-1} s^{-1}$) to the parent pentacene (1.4 $cm^2 V^{-1} s^{-1}$). Such a high performance is comparable with other related materials, such as triisopropylsilylethynylpentacene (>1 $cm^2 V^{-1} s^{-1}$),[24–26] alkylated dinaphtho[2,3-*b*:2′,3′-*f*]thieno[3,2-*b*]thiophenes (>10 $cm^2 V^{-1} s^{-1}$),[27,28] and the crystal of tetracene analogous of rubrene (>18 $cm^2 V^{-1} s^{-1}$).[29,30] In previous reports, the charge mobility of hexacene and derivatives were measured in the devices either made with single crystals,[21] or with crystalline thin films prepared through solution method.[22,31] However, the physical properties and transistor characteristics of hexacene thin film that is prepared by vacuum deposition method have not yet been reported.

It is believed that the bromine substituent can provide a suitable size to improve crystal packing. Judged by the past high-performance of brominated tetracene and pentacene, it is therefore in demand to explore the possibility of brominated analogue of hexacene. In this regard, the brominated analogue of hexacene, *i.e.*, 2-bromohexacene (**1a**), is synthesized and its charge-transport property is examined. Precursor **2a** is cleanly converted to **1a** by thermal decomposition, and **1a** exhibits high thermal stability in the dark over 90 days (Fig. 1). This is the first example of the charge-transport property of a stable vacuum-deposited thin-film of hexacene and halogenated hexacene for electronic devices.

2. Results and discussion

2.1. Synthesis

The synthesis of **2a** is shown in Scheme 1. Dimethylfulvene derivative **3** and benzoquinone **4** were treated with *s*-tetrazine, affording diketone **5** as an *endo–exo* mixture, then the double bond of **5** was reduced using zinc in acetic acid, affording adduct **6**. The aldol reaction of **6** with dialdehyde **7** afforded diketone **8** as an *endo* compound in 17% yield (from **3**, three steps). Pure *endo*-**8** was crystallized probably due to steric influence by the bromo-substituent. It was reduced by $NaBH_4$, and further treatment with $POCl_3$/pyridine afforded aromatic compound **9** in 48% yield (from **8**, two steps). The *exo*-double bond was treated with OsO_4 to give a diol, followed by treatment

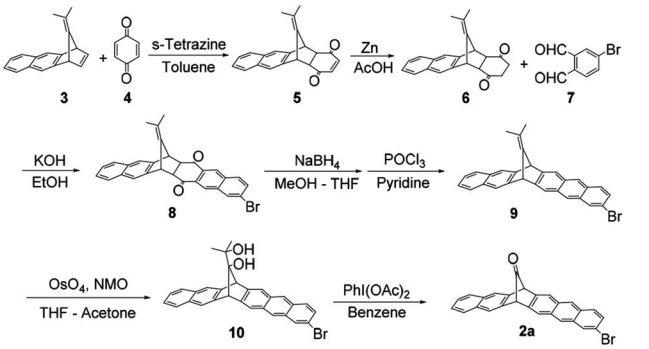

Scheme 1 Synthetic route of **2a**.

with $PhI(OAc)_2$ to give desired **2a** in 31% yield. The total yield was 2.5% in 7 steps.

The absorption spectrum of **2a** in 1,2,4-trichlorobenzene exhibited characteristic ^1A–^1L_a transitions of the anthracene chromophore at 353, 371, 391 and 408 nm, with vibrionic progressions, which were red-shifted from the peaks of parent **2b** at 350, 368 and 391 nm in the 1,2,4-trichlorobenzene solution (Fig. S1†). When the solution of **2a** was heated at 230 °C, the solution changed from colorless to pale-green, which exhibited characteristic acene vibration absorption bands at 573, 623 and 679 nm. However, this colour changed to yellow within a few minutes owing to the dimerization or oxidation of **1a**.

2.2. Physical properties

The absorption maximum in the visible range was observed at 679 nm, whereas parent hexacene **1b** exhibited the peak maximum at 675 nm in 1,2,4-trichlorobenzene (Fig. S1†). The peaks were red-shifted from those of parent hexacene **1b** by 4 nm, indicating the reduction of HOMO–LUMO gap of **1a** by the bromo substituent. This phenomenon has similarly been observed in the pairs of tetracene (473 nm in THF) and 2-bromotetracene (477 nm in THF),[22] as well as pentacene (575 nm in THF) and 2-bromopentacene (578 nm in THF).[23] To compare with the reported hexacene analogues, the peak maximum was shown to be red-shifted from that of pentaceno[2,3-*b*]thiophene (640 nm in *o*-DCB)[30] due to the increase of aromaticity. In comparison with other substituent group effect, however, it showed a blue shift from those of tricyclohexylsilylethynyl-octafluorohexacene (725 nm),[31] tri-*tert*-butylsilylethynyl-hexacene (738 nm),[32,33] and trialkylsilylethynyl-azahexacene (825–842 nm in hexane)[34] due to the electron-donating effect of the trialkylsilylethynyl acetylene units.

In the thermal gravimetric analysis (TGA) profile of **2a**, the first weight loss (8.5%, calcd 6.5%) was observed at approximately 200 °C to generate **1a**. The thermal weight loss profile did not change up to 360 °C. Then it was followed by the second weight loss caused by the vaporisation as well as the decomposition of **1a** at temperatures greater than 400 °C (Fig. 2a). Decarbonylation at 200 °C was confirmed by infrared (IR) spectroscopy, which revealed the disappearance of the characteristic C=O stretching band at 1786 cm^{-1} after heating at 230 °C (Fig. 2b). The high-resolution FAB-MS spectrum revealed

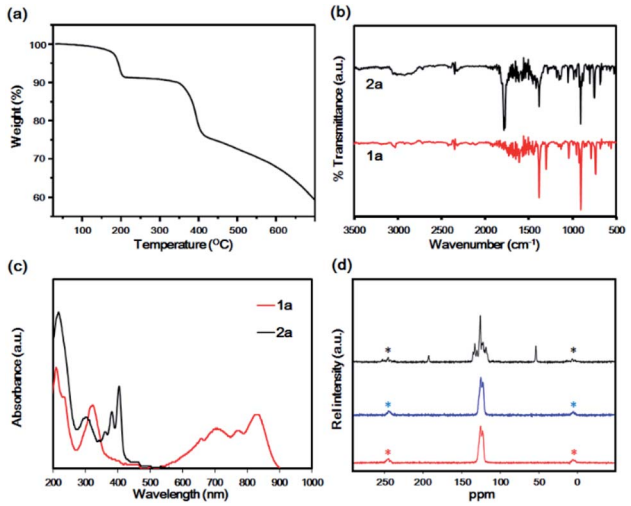

Fig. 2 (a) TGA profile of **2a** under nitrogen. Heating rate was 10 °C min^{-1}. (b) IR spectra of **2a** (black) and after heating at 230 °C for conversion to **1a** (red) under ambient conditions. (c) Reflectance absorption spectra of drop-casted **2a** on a quartz plate (black) and after heating at 230 °C for conversion to **1a** (red) under ambient conditions. (d) Solid-state ^{13}C CP-MAS spectra of **2a** (black), **1a** (blue) and **1a** after 90 days in the dark (red). The asterisk denotes the spinning side band.

a molecular ion signal at *m*/*z* 406.0387 (M+, calcd 406.03571, error = +7.4 ppm), which corresponded to **1a**. The purity was also confirmed by correct elemental analysis. The absorption spectra of **2a**, fabricated by drop-casting a saturated chlorobenzene solution on a quartz substrate, exhibited a similar vibration structure to that of **2a** in solution, with characteristic peaks at 403, 380 and 364 nm, indicative of the fabrication of film of **2a**. In contrast, after heating at 230 °C under nitrogen, a broad band was observed at 500–900 nm, and the peaks at 360–400 nm, which are characteristic of the anthracene moiety, disappeared.

These structures were different from that of **1a** in solution. Film **1a** exhibited characteristic peaks at 833 and 776 and at 708 and 661 nm. These peaks exhibited the appearance of Davydov splitting effect.[20,21,35] The same pattern appeared in other related acene structures in the solid state, including parent **1b**, at 840 nm, 765 nm, 708 nm and 654 nm.[20] The first bands at 833 and 775 nm corresponded to the 0–0 band, and those at 708 and 654 nm corresponded to the 0–1 band (Fig. 2c). The high thermal stability of **1b** in the solid state was confirmed by solid-state NMR that maintained invariant over 1 month.[13] Comparing it with heptacene under a similar situation, the latter dimerised slightly after 1 month.[16] To verify the thermal stability of **1a**, ^{13}C CP-MAS NMR spectra were recorded for monitoring the variation of the carbon skeleton. Compound **2a** exhibited three main peaks at 193.2 (bridge position of C=O), 137–114 (aromatic carbon atoms) and 54.4 ppm (bridgehead tertiary carbon atom). After the conversion to **1a**, the spectrum exhibited aromatic carbon peaks at 125.7 and 122.9 ppm only, indicating a quantitative transformation. After maintaining **1a** for 90 days in the dark under air atmosphere, no changes were observed in the CP-MAS spectrum, indicative of the high thermal stability of **1a** (Fig. 2d). This high thermal stability can be compared with the reported property of hexacene (>1 month in dark)[20] and tricyclohexylsilylethynylhexacene (several month).[33] The film of **1a** was grown by vacuum sublimation and exhibited a structure similar to the film in Fig. 2c (Fig. S3†). The ionisation potential (E_{ip}) and electron affinity (E_{ea}) of the film **1a** were −5.24 and −3.30 eV, respectively, while those of **1b** were −4.81 and −2.70 eV, respectively (Fig. S4†). The E_{ip} of thin film **1b** (−4.81 eV) was consistent with that of the crystalline powder reported previously (−4.96 eV).[14] The energy gap of **1a** (1.94 eV) was less than that of **1b** (2.11 eV). Theoretical computation results (DFT, B3LYP/6-31G(d) level) revealed the HOMO and LUMO of **1b** to be −4.68 and −2.90 eV, respectively, while the corresponding values for **1a** were −4.81 eV and −3.04 eV, respectively. The HOMO and LUMO were lowered by bromination compared with those of **1a**, indicative of the electron-withdrawing effect by the bromo substituent. The HOMO–LUMO gap of **1a** was 1.77 eV, whereas that of **1b** was 1.78 eV, supporting the experimental results (Table 1).

2.3. Charge transport properties

The properties of organic field-effect transistors (OFETs) made with the films of **1a–b** were examined. The OFET devices were fabricated by vacuum sublimation of **1a–b** under a pressure of 8 × 10^{-6} torr to deposit the thin films on an HMDS/SiO_2/Si substrate, followed by the deposition of gold electrodes on the top of the films. The film thickness of **1a–b** was 60 nm. The channel dimension of the source/drain electrodes was 45 × 2000 μm. The output parameters were measured on a selected film across a source–drain channel, followed by the plot of drain current (I_D) *versus* drain source voltage (V_{DS}) at various gate voltages (V_G). The corresponding transfer characteristics were plotted for log(I_D) *versus* V_G at a V_{DS} of −100 V and I_D *versus* V_{DS}

Table 1 Physical properties of **1a–b**

Sample	Ionization potential (E_{ip}, eV)[a]	Electron affinity (E_{ea}, eV)[b]	Energy gap (eV)[c]	Optical gap (eV)[d]	HOMO (E_H, eV)[e]	LUMO (E_L, eV)[e]	Energy gap (eV)[f]	Reorganization energy (λ^+, meV)[e]
1a	−5.24	−3.30	1.94	1.47	−4.81	−3.04	1.77	85
1b	−4.81	−2.70	2.11	1.41	−4.68	−2.90	1.78	79

[a] Estimated by photoelectron yield spectroscopy. [b] Estimated by low-energy inverse photoemission spectroscopy. [c] $E_{ip} - E_{ea}$. [d] Estimated by the edge of absorption spectra of thin-film. [e] B3LYP/6-31G(d). [f] $E_H - E_L$.

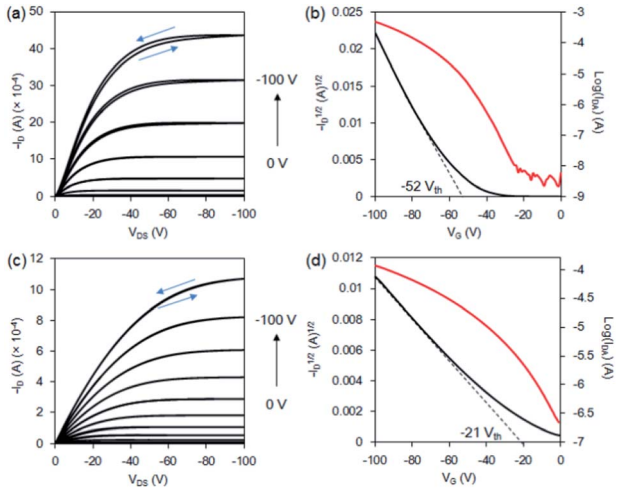

Fig. 3 Vacuum-deposited thin-film OFET made using **1a**. (a) Output characteristics, where D and S are the drain and source, respectively. (b) Transfer characteristics recorded at $V_{DS} = -100$ V, where G is the gate, and the vacuum-deposited thin-film OFET was made using **1b**. (c) Output characteristics, where D and S are the drain and source, respectively. (d) Transfer characteristics recorded at $V_{DS} = -100$ V, where G is the gate.

in the saturation mode. The field-effect hole mobility of **1a** was measured, and the mobility values ranged from 0.21 to 0.83 cm^2 V^{-1} s^{-1} with threshold voltages of −50 to −69.3 V. The averaged performance of six independent devices was 0.52 cm^2 V^{-1} s^{-1} and a threshold of −56.3 V. The best mobility of bromohexacene **1a** was observed at 0.83 cm^2 V^{-1} s^{-1} with an on/off ratio of 5.0 × 10^4 and a threshold of −52 V (Fig. 3a–b). To compare the hole mobility, parent **1b** was also tested. The mobility of **1b** in the saturation mode ranged from 0.072 to 0.076 cm^2 V^{-1} s^{-1} with a threshold voltage ranging from −19 to −22 V. The averaged performance of six independent devices was 0.074 cm^2 V^{-1} s^{-1} and a threshold of −20.7 V. The best film mobility of **1b** was observed at 0.076 cm^2 V^{-1} s^{-1} with an on/off ratio of 2.4 × 10^2 and a threshold of −21 V (Fig. 3c–d). Previously, the hole mobility of hexacene **1b** has been reported in the single-crystal phase and in the spin-coated thin-film phase by the precursor method. The best hole-transfer mobility by spin-coated **1b** was 0.035 cm^2 V^{-1} s^{-1}, with a similar surface treatment on SiO_2/Si substrate. Although our fabrication conditions were not fully optimised, the mobility of the vacuum-deposited film was greater than that of the spin-coated one. It indicates that better crystalline films of **1b** were formed by thermal deposition. The mobility of film **1a** exhibited a larger range of randomness compared to **1b**. However, a higher hole-transfer efficiency of **1a** ranging 7- to 10-folds compared with that of **1b** was observed in all tested devices. This result indicated that the packing moiety and/or film morphology possessing a better charge-transfer pathway may account for the mobility. Previously, a single-crystal bromopentacene was found to exhibit a 4-fold faster hole-transfer speed than that of non-substituted pentacene, while their reorganization energies were estimated to be 102 meV and 95 meV (B3LYP/6-31Gd level), respectively.[23]

DFT computations revealed that the reorganisation energy between the radical cation and ground state of **1a** was 85 meV (B3LYP/6-31Gd level). This value was quite close to that of **1b** (79 meV), suggesting a similar energy loss during structure reorganization in the hexacenes **1a** and **1b**.

2.4. TEM, XRD, and AFM measurements of hexacene films

To investigate the morphology of thin-film, we performed a surface analysis on the films **1a** and **1b**. Fig. 4 showed cross-section of transmission electron microscope (TEM) image of *ca.* 60 nm deposited films **1a** and **1b** on HMDS/SiO_2/Si surface. The ion milling method allows us to examine a cross-section of substrate at the interface of **1a–b** and HMDS/SiO_2/Si. The TEM image show a good continuous growth of **1a** and **1b** films on HMDS/SiO_2/Si surface, suggesting both films were deposited uniformly on the substrate.

The parent structure of hexacene **1b** exhibited a herringbone arrangement, where the face-to-edge stacking arrangement between adjacent molecules avoided the progress of dimerization and led to a high thermal stability in the solid state.[14] The vacuum-deposited film of **1b** exhibited out-of-plane X-ray diffraction (XRD) peaks along (00*l*) direction and in-plane XRD along (*hk*0) direction (Fig. S4†).

These patterns indicated that the molecules in the deposited film are oriented vertical to the surface along their long axis. In addition, this film orientation was consistent with the reported out-of-plane pattern of heat-converted film **1b** from corresponding precursor compound.[21] The (001) peak was observed at 4.84° corresponding to an interplanar distance of 18.3 Å. This value can be compared with the *d*-spacing in the single crystal of **1b**, which has been estimated to be 16.4 Å. It indicates that the molecules in the crystalline film **1b** are tilted on the surface of HMDS/SiO_2/Si substrate. The out-of-plane and in-plane XRD peaks of vacuum-deposited film **1a** exhibited (00*l*) and (*hk*0) patterns, indicating that molecules in film **1a** is oriented along the long axis normal to the surface (Fig. S4†). Although film **1a** exhibited weaker XRD diffraction peaks compared with that of **1b**, the 2θ angle of **1a** observed at a smaller angle of 4.43° on the HMDS/SiO_2/Si substrate. The *d*-spacing of bromohexacene molecules is estimated to be 20.0 Å. The larger *d*-spacing revealed that the molecules interact through the *a*–*b* axis.

To further study of finding the difference of mobility between **1a** and **1b**, the atomic force microscope (AFM) analysis was investigated. The films **1b** revealed a high surface roughness of 12.01 nm (Fig. 5). In contrast, film **1a** revealed a lower roughness of 6.48 nm. This smoother

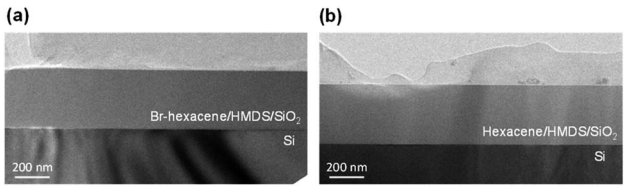

Fig. 4 TEM image of thin films **1a** (a) and **1b** (b). Top: structure of films on HMDS/SiO_2/Si.

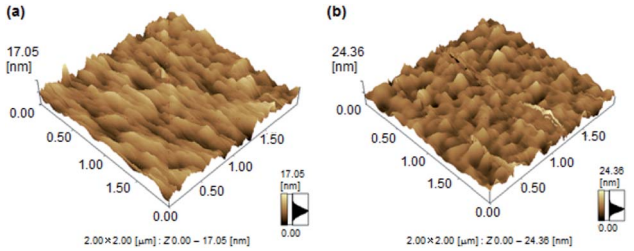

Fig. 5 AFM images of thin films of **1a** and **1b**.

surface in **1a** achieved a small energy loss during the transport of holes between the source and drain.

3. Materials and methods

3.1. General information

The ^{1}H and ^{13}C NMR spectra were recorded in solutions on a BrukerAV600 (600 MHz) spectrometer. The ^{1}H and the ^{13}C NMR chemical shifts were reported as δ values (ppm) relative to external Me_4Si. The coupling constants (J) were given in hertz. High resolution FAB mass spectra were recorded on a JMS-700 MStation spectrometer. FAB MS spectra were measured with 3-nitrobenzyl alcohol (NBA) as the matrix. Analytical thin layer chromatography (TLC) was performed on silica gel 60 F_{254} Merck. Column chromatography was performed on KANTOSi60N (neutral). Absorption and reflectance spectra were recorded on a SHIMADZU UV-3600. IR spectra were performed by SHIMADZU IRPrestige-21 spectrophotometer. AFM measurements were tested by SHIMADZU SPM-9700. The elemental analyses were recorded on a Yanaco CHN recorder MT-6. THF was distilled from sodium benzophenon ketyl. Toluene was distilled from CaH_2. Other solvents and reagents were of reagent quality, purchased commercially, and used without further purification.

3.2. ^{13}C CP/MAS NMR

The ^{13}C CP/MAS NMR spectra were acquired with a Bruker Avance 400 MHz NMR spectrometer, equipped with a 4 mm double resonance probe operating at the ^{1}H and the ^{13}C Larmor frequencies of 400.13 and 100.63 MHz, respectively. For the polarization transfer, the contact-time was set to 1.75 ms. During data acquisition, ^{1}H decoupling by spinal-64 was applied. Powdered samples were packed in 4 mm zirconium oxide MAS rotors with Kel-F cap. A sample spinning frequency of 12 kHz was used and regulated by a spinning controller within $\pm$1 Hz. All CP-MAS experiments were carried out at ambient temperature. The ^{13}C NMR chemical shifts are referenced to the methyl signal (=17.36 ppm) of hexamethylbenzene, which was used as an external standard. All measurements were performed in air, and the sample tube was kept in the dark between measurements.

3.3. FET measurement

The electrical measurements were carried out in vacuum using a semiconductor parameter analyzer (B1500A, Keysight). The saturation mobility (μ_{sat}) was extracted from the slope of the square root of the drain current plot *vs.* V_G from eqn (1).

$$I_{D,sat} = \frac{W}{2L} C_i \mu_{sat} (V_G - V_T)^2 \quad (1)$$

where $I_{D,sat}$ is the drain-to-source saturated current; W/L is the channel width to length ratio; C_i is the capacitance of the insulator per unit area, and the V_G and V_T are gate voltage and threshold voltage, respectively. A heavily doped silicon (Si) wafer was used for a back gate electrode, which was covered with a 300 nm-thick thermally grown SiO_2 (C_i = 10.2 nF cm^{-2}) as the gate insulator. Channel length (L) and width (W) were 2000 μm and 45 μm.

3.4. TEM measurement

The organic films were vacuum sublimation of **1a–b** under a pressure of 8×10^{-6} torr to deposit the thin films for 350 nm on a HMDS/SiO_2/Si substrate. Cross-sectional TEM samples for all of the films were prepared by mechanical thinning and ion milling. The transmission electron microscope used in this study was a JEOL JEM-2100F, which was operated at an accelerating voltage of 200 kV.

3.5. Synthesis of materials

3.5.1. Synthesis of (6 *aS*,14*aR*,15*S*)-10-bromo-17-(propan-2-ylidene)-6,6*a*,14*a*,15-tetrahydro-6,15-methanohexacene-7,14-dione 8. A solution of 1*R*,4*S*-11(propan-2-ylidene)-1,4-dihydro-1,4-methanoanthracene **3** (232 mg, 1.00 mmol), benzoquinone **4** (108 mg, 1.00 mmol), and 3,6-bis(2-pyridyl)tetrazine (248 mg, 1.05 mmol) in toluene (50 mL) was heated at 95 °C for 24 h under a nitrogen atmosphere. After the reaction, the mixture was quenched with 30% H_2SO_4, extracted with CH_2Cl_2, and the organic solution was dried over $MgSO_4$ and concentrated *in vacuo*. The crude product was purified by a silica gel chromatograph eluted with CH_2Cl_2 to afford a mixture of *endo* and *exo* geometrical isomers of **5** (163 mg) as yellow solids. The mixture was used for next step without further purification.

The mixture of **5** (163 mg, 0.519 mmol) and zinc (600 mg) and glacial acetic acid (50 mL) was sonicated for 30 min at room temperature. After reaction, the suspension was filtered and the solution was evaporated to give the crude product. Silica gel chromatography of the crude product with CH_2Cl_2 and treatment with iced MeOH afforded dione **6** (114 mg). The mixture was used for next step without further purification.

A mixture of diketone **6** (114 mg, 0.361 mmol) and 4-bromophthalaldehyde **7** (76.1 mg, 0.361 mmol) was dissolved in EtOH (50 mL). The EtOH solution was bubbled by nitrogen gas for 20 min to remove oxygen. To the mixture was added 10 wt% KOH/EtOH solution (2–3 drops) in the nitrogen atmosphere and stirred 72 h at room temperature under nitrogen gas. The mixture gradually became dark, and pale-yellow powder precipitated. After reaction, the precipitate was filtered and washed with EtOH and hexane to afford *endo*-**8** (86.2 mg, 17% in three steps). Pale yellow powder (EtOH). δ_H ($CDCl_3$, 600 MHz) 1.23 (d, J = 4.8, 6H), 3.17 (s, 2H), 4.47 (s, 2H), 7.45 (dd, J = 6.0, 3.0 Hz, 2H), 7.76 (J = 9.0, 7.7 Hz, 1H), 7.78 (s, 2H), 7.82 (dd, J =

6.0, 2.4 Hz, 2H), 7.95 (d, $J = 8.4$ Hz, 2H), 8.24 (s, 1H), 8.53 (s, 1H), 8.61 (s, 1H). δ_C ($CDCl_3$, 125 MHz) 19.7, 51.3, 52.9, 117.9, 119.0, 124.1, 125.6, 127.5, 127.9, 128.6, 131.4, 131.9, 132.2, 132.8, 132.9, 133.5, 136.0, 142.3, 143.7, 197.0, 197.8.

3.5.2. Synthesis of (6*S*,15*R*)-10-bromo-17-(propan-2-ylidene)-6,15-dihydro-6,15-methanohexacene 9. To a solution of dione **8** (220 mg, 0.446 mmol) in MeOH (50 mL) and THF (50 mL) in an ice bath was added $NaBH_4$ (74 mg, 1.65 mmol). After 2 h, the reaction mixture was quenched with water. The aqueous solution containing precipitates was extracted with CH_2Cl_2. The organic layer was washed with water, and dried over anhydrous $MgSO_4$. Removal solvent gave the diol **9** (212 mg) as yellow solids. This crude compound was subjected to the next step without further purification. To a mixture of diol **9** and dried pyridine (10 mL) was added dropwise $POCl_3$ (0.9 mL) at 0 °C. The resulting mixture was stirred at room temperature for 72 h, then at 80 °C for another 30 min. The mixture was poured into ice water and was extracted with CH_2Cl_2. The organic layer was washed successfully with 3 N HCl and brine, then was dried over $MgSO_4$. The crude product was purified by a silica gel chromatograph eluted with hexane/CH_2Cl_2 (4 : 1) to give the aromatized compound **9** (98.8 mg, 48%) as pale yellow powder. Physical data of **9**: pale yellow powder (EtOH). δ_H ($CDCl_3$, 600 MHz) 1.72 (s, 6H), 5.06 (s, 2H), 7.35 (dd, $J = 6.0$, 3.0, 2H), 7.43 (dd, $J = 9.0$, 7.2 Hz, 1H), 7.70 ($J = 6.0$, 3.0 Hz, 2H), 7.72 (s, 2H), 7.77–7.79 (m, 3H), 8.08 (s, 1H), 8.12 (s, 1H), 8.19 (s, 1H). δ_C ($CDCl_3$, 125 MHz) 19.8, 51.4, 113.2, 118.3, 118.4, 118.9, 119.0, 119.02, 124.9, 125.5, 126.1, 127.7, 128.3, 129.6, 131.3, 131.7, 132.2, 132.4, 145.2, 145.3, 145.6, 153.8.

3.5.3. Synthesis of (6*S*,15*R*)-10-bromo-6,15-dihydro-6,15-methanohexacen-17-one 2a. A mixture of olefin **9** (200 mg, 0.433 mmol) and *N*-methylmorpholine *N*-oxide (NMO) (50% in H_2O, 1.5 mL) in a mixed solvent of acetone (50 mL) and H_2O (1.5 mL) was stirred at room temperature until **9** was dissolved completely. To the solution was added a few drops of OsO_4 (4% H_2O soln). The reaction was monitored by TLC until completion, then the mixture was quenched with 15% aqueous $Na_2S_2O_4$. The aqueous solution was extracted with EtOAc, dried over Na_2SO_4, and evaporated. The product was purified by a silica gel chromatograph eluted with CH_2Cl_2 to give diol **10** (79 mg), which was directly used in the next step. The diol **10** (79 mg) and $PhI(OAc)_2$ (120 mg) in benzene (100 mL) was stirred at 60 °C for 12 h. After reaction, the mixture was cooled in an ice bath, while white precipitates formed. The solids were collected by suction filtration to give compound **2a** (59 mg, 31% in two steps) as a white powder. Physical data of **2a**: m.p. 181 °C. (TGA, decomp.); IR (KBr): ν 1786 cm^{-1} (s, C=O); ^{13}C CP/MAS NMR (12 000 rpm, 100 MHz): 54.0, 118.5, 120.6, 122.5, 123.9, 126.1, 130.5, 133.2, 135.2, 192.7.

3.5.4. Synthesis of 2-bromohexacene 1a. Proper amount of precursor **2a** was loaded in a glass container, and the powder was heated at 210 °C for 5 min under a nitrogen atmosphere. The color of **2a** changed from white to green to give 2-bromohexacene **1a** in a quantitative yield. M.p. 340 °C. (TGA, sublime); ^{13}C CP/MAS NMR (12 000 rpm, 100 MHz): 123.1, 126.0; HRMS: *m*/*z* 406.0387 (M+, calcd 406.03571); EA: found, %: C, 76.2; H, 3.7. For $C_{26}H_{15}Br$. Calculated, %: C, 76.1; H, 3.7.

4. Conclusions

A novel hexacene precursor was successfully synthesised, which can be quantitatively converted at around 200 °C to the corresponding 2-bromohexacene. It exhibited high thermal stability over 3 months in the dark. The bromine atom affected the hexacene crystal packing and decreased the HOMO–LUMO energy gap. The thin-film of **1a** was fabricated by using both spin-coating and vacuum sublimation methods, and both films exhibited exciton coupling, indicative the presence of herringbone arrangement in the polycrystalline film. The film of **1a** exhibited a more efficient hole-transport property compared with that of parent **1b**. Hence, film **1a** exhibits a higher hole mobility of 0.83 $cm^2 V^{-1} s^{-1}$ than that of **1b** (0.074 $cm^2 V^{-1} s^{-1}$). Although these hole mobility were lower than that of single crystal hexacene (4.28 $cm^2 V^{-1} s^{-1}$),[26] it was comparable with the reported value of solution-processed single crystal tricyclohexylsilylethynyloctafluorohexacene (0.1 $cm^2 V^{-1} s^{-1}$).[31] To the best of our knowledge, this is the first study on the charge-transport property of a stable vacuum-deposited thin-film of hexacene for electronic device. Currently, other derivatives of halogenated hexacene are prepared, and their properties related to optoelectronic devices are being examined. The results will be reported in due course.

Author's contributions

MW designed and performed the experiments and theoretical calculations; TM, CTC, MS and SSS were synthesized, measured and analysed the materials and physical properties; TM and CA designed the devices and analysed the data; JM measured and analysed the TEM; MW and TI were measured and analysed the NMR data; MW, TM and TJC were co-wrote the manuscript; all authors gave final approval for publication.

Conflicts of interest

There are no conflicts to declare.

Acknowledgements

This work was supported by a Grant-in-Aid for Science Research (JP17H04888, JP17K19123) from the Ministry of Education, Culture, Sports, Science and Technology (MEXT), Japan, and was performed under the Cooperative Research Program of "Network Joint Research Centre for Materials and Devices (IMCE, Kyushu University)". The computation was mainly carried out using the computer facilities at Research Institute for Information Technology, Kyushu University. MW and TM acknowledge support from I2CNER, funded by the World Premier International Research Centre Initiative (WPI), Ministry of Education, Culture, Sports, Science and Technology of Japan (MEXT), Japan. TJC and SSS are also grateful for the supports from the Ministry of Science and Technology of Taiwan and Academia Sinica.

Notes and references

1 Q. Ye and C. Chi, *Chem. Mater.*, 2014, **6**, 4046.
2 M. Bendikov, H. M. Duong, K. Starkey, K. N. Houk, E. A. Carter and F. Wudl, *J. Am. Chem. Soc.*, 2004, **126**, 7416.
3 Y. Yang, E. R. Davidsonb and W. Yang, *Proc. Natl. Acad. Sci.*, 2016, **113**, E5098.
4 J. Mei, Y. Diao, A. L. Appleton, L. Fang and Z. Bao, *J. Am. Chem. Soc.*, 2013, **135**, 6724.
5 K. Takimiya, S. Shinamura, I. Osaka and E. Miyazaki, *Adv. Mater.*, 2011, **23**, 4347.
6 J. E. Anthony, *Angew. Chem., Int. Ed.*, 2008, **47**, 452.
7 J. Krüger, F. Garcia, F. Eisenhut, D. Skidin, J. M. Alomso, E. Guitián, D. Pérez, G. Cuniberti, F. Moresco and D. Peña, *Angew. Chem., Int. Ed.*, 2013, **52**, 3810.
8 Q. Miao, *Adv. Mater.*, 2014, **26**, 5541.
9 K. Aryanpour, A. Shukla and S. Mazumdar, *J. Phys. Chem. C*, 2015, **119**, 6966.
10 B. Purushothaman, M. Bruzek, S. R. Parkin, A.-F. Miller and J. E. Anthony, *Angew. Chem., Int. Ed.*, 2011, **50**, 7013.
11 A. Maliakal, K. Raghavachari, H. Katz, E. Chandross and T. Siegrist, *Chem. Mater.*, 2004, **16**, 4980.
12 S. S. Zade and M. Bendikov, *J. Phys. Org. Chem.*, 2012, **25**, 452.
13 M. Watanabe, K. Y. Chen, Y. J. Chang and T. J. Chow, *Acc. Chem. Res.*, 2013, **46**, 1606.
14 M. Suzuki, T. Aotake, Y. Yamaguchi, N. Noguchi, H. Nakano, K. Nakayama and H. Yamada, *J. Photochem. Photobiol., C*, 2014, **18**, 50.
15 C. Tönshoff and H. F. Bettinger, *Angew. Chem., Int. Ed.*, 2010, **49**, 4125.
16 R. Einholz, T. Fang, R. Berger, P. Grüninger, A. Früh, T. Chassé, R. F. Fink and H. F. Bettinger, *J. Am. Chem. Soc.*, 2017, **139**, 4435.
17 T. Yelin, R. Korytár, N. Sukenik, R. Vardimon, B. Kumar, C. Nuckolls, F. Evers and O. Tal, *Nat. Mater.*, 2016, **15**, 444.
18 S. R. Yost, J. Lee, M. W. B. Wilson, T. Wu, D. P. McMahon, R. R. Parkhurst, N. J. Thompson, D. N. Congreve, A. Rao, K. Johnson, M. Y. Sfeir, M. G. Bawendi, T. M. Swager, R. H. Friend, M. A. Baldo and T. V. Voorhis, *Nat. Chem.*, 2014, **6**, 492.
19 E. Busby, T. C. Berkelbach, B. Kumar, A. Chernikov, Y. Zhong, H. Hlaing, X.-Y. Zhu, T. F. Heinz, M. S. Hybertsen, M. Y. Sfeir, D. R. Reichman, C. Nuckolls and O. Yaffe, *J. Am. Chem. Soc.*, 2014, **136**, 10654.
20 M. Watanabe, Y. J. Chang, S.-W. Liu, T.-H. Chao, K. Goto, M. M. Islam, C.-H. Yuan, Y.-T. Tao, T. Shinmyozu and T. J. Chow, *Nat. Chem.*, 2012, **4**, 574.
21 M. Watanabe, W.-T. Su, K.-Y. Chen, C. T. Chien, T.-H. Chao, Y. J. Chang, S.-W. Liu and T. J. Chow, *Chem. Commun.*, 2013, **49**, 2240.
22 M. Watanabe, T.-H. Chao, C.-T. Chien, S.-W. Liu, Y. J. Chang, K.-Y. Chen and T. J. Chow, *Tetrahedron Lett.*, 2012, **53**, 2284.
23 C.-T. Chien, M. Watanabe and T. J. Chow, *Tetrahedron*, 2015, **71**, 1668.
24 H. Sirringhaus, *Adv. Mater.*, 2014, **26**, 1319.
25 Y. Diao, B. C.-K. Tee, G. Giri, J. Xu, D. H. Kim, H. A. Becerril, R. M. Stoltenberg, T. H. Lee, G. Xue, S. C. B. Mannsfeld and Z. Bao, *Nat. Mater.*, 2013, **12**, 665.
26 M. J. Kang, I. Doi, H. Mori, E. Miyazaki, K. Takimiya, M. Ikeda and H. Kuwabara, *Adv. Mater.*, 2011, **23**, 1222.
27 K. Nakayama, Y. Hirose, J. Soeda, M. Yoshizumi, T. Uemura, M. Uno, W. Li, M. J. Kang, M. Yamagishi, Y. Okada, E. Miyazaki, Y. Nakazawa, A. Nakao, K. Takimiya and J. Takeya, *Adv. Mater.*, 2011, **23**, 1626.
28 J. Takeya, M. Yamagishi, Y. Tominari, R. Hirahara and Y. Nakazawa, *Appl. Phys. Lett.*, 2007, **90**, 102120.
29 C. Reese, W.-J. Chung, M.-M. Ling, M. Roberts and Z. Bao, *Appl. Phys. Lett.*, 2006, **89**, 202108.
30 M. L. Tang, S. C. B. Mannsfeld, Y.-S. Sun, H. A. Becerril and Z. Bao, *J. Am. Chem. Soc.*, 2009, **131**, 882.
31 B. Purushothaman, S. R. Parkin, M. J. Kendrick, D. David, J. W. Ward, L. Yu, N. Stingelin, O. D. Jurchescu, O. Ostroverkhova and J. E. Anthony, *Chem. Commun.*, 2012, **48**, 8261.
32 M. M. Payne, S. R. Parkin and J. E. Anthony, *J. Am. Chem. Soc.*, 2005, **127**, 8028.
33 B. Purushothaman, S. R. Parkin and J. E. Anthony, *Org. Lett.*, 2010, **12**, 2060.
34 B. D. Lindner, J. U. Engelhart, O. Tverskoy, A. L. Appleton, F. Rominger, A. Peters, H.-J. Himmel and U. H. F. Bunz, *Angew. Chem., Int. Ed.*, 2011, **50**, 8588.
35 Q. Miao, T.-Q. Nguyen, T. Someya, G. B. Blanchet and C. Nuckolls, *J. Am. Chem. Soc.*, 2003, **125**, 10284.